

# Topological pseudogap in systems with strong electron-phonon interaction and cuprates-like dispersion

S. V. Doronkina, A. E. Myasnikova, A. H. Dzhantemirov, A. V. Lutsenko

Southern federal university, Rostov-on-Don, Russia

E-mail: myasnikova67@yandex.ru

Pseudogap in doped cuprates is seemingly as enigmatic as superconductivity in them. We study Bloch states reconstruction under influence of potential created by charge ordering (CO) that emerges in doped systems with strong Frohlich electron-phonon interaction. In such systems carriers with energies near minimal one form large polarons and bipolarons which, in turn, organize in unconventional charge density wave. To describe an impact of its potential on delocalized carriers we develop an approach combining Wannier theorem and a method reminiscent of finite elements one. We show that quasiparticle in such systems represents “distributed wave packet” having different momentums in regions with different CO potential and topology of cuprates-like dispersion makes impossible propagation of quasiparticles with average momentum near antinode. Antinodal photoelectrons stem from quasiparticles with average momentum rather far from antinode, when they escape from regions with high negative CO potential. As a result, the energies of antinodal photoelectrons is by the CO potential amplitude lower than ones dictated by dispersion for their momentums. Therefore near-antinodal spectral weight in ARPES spectra of the considered system experiences shift of the order of CO potential amplitude to higher binding energies, appearing also at momentums well above Fermi crossing but at energies well below Fermi energy, and great broadening due to uncertainty of the quasiparticle momentum. Just such pseudogap peculiarities are characteristic of near-antinodal ARPES spectra in cuprates at low temperatures corresponding to CO presence.

**Keywords:** pseudogap, cuprates, charge ordering, electron-phonon interaction, large bipolaron, ARPES spectra

## Introduction

33 years of studying high-temperature superconductors resulted in great advance in experimental methods and finding many unique properties of cuprates as well as discovering high-temperature superconductivity (HTSC) in new classes of materials including pnictides and interfacial HTSC [1]. However, decisive progress in theoretical calculation of the transition temperature or understanding the nature of unusual phases of doped cuprates like pseudogap or strange metal phases [2] was not reached. A possible way to overcome this problem is to take into account other interactions present in cuprates besides electron correlations [2], in particular, electron-phonon interaction (EPI) which allows to introduce into the theory dependence of the system properties on its structure [3].

Softening of optical phonon modes with the wave vectors near the CO one [4,5] (theoretical calculation of the CO wave vector in the model with strong EPI is carried out in [6]), and wide bands in ARPES and optical spectra [7-15] are ordinarily considered as fingerprints of strong EPI in cuprates. Local density of states modulation due to coupling to the  $B_{1g}$  phonon mode observed in inelastic tunneling spectra [16] and current fluctuations observed with scanning noise spectroscopy [17] represent new experimental evidences of strong EPI in cuprates. The discovery of HTSC with  $T_c = 109K$  at the interface of a monomolecular FeSe layer epitaxially grown on a  $SrTiO_3$  substrate [18-20] has contributed to understanding the importance of taking EPI into account when studying the nature of HTSC. Indeed, on the one hand, strong EPI is characteristic of strontium titanate, on the other hand, properties of the new interface

superconductor are very different from those predicted in the framework of an approach that takes into account only electronic correlations [1]. Since constructing a new theory for each type of high-temperature superconductors is not very attractive [1], we try to take into account, in addition to electronic correlations, the role of the crystal lattice (in particular, EPI) for more unified description of properties of these systems [1, 21].

Electronic correlations that determine the band structure of cuprates are ordinarily considered in the nodal representation, therefore it is technically easier to add to them strong short-range (Holstein) EPI [10,11,22,23]. However, such EPI leads to the formation of small polarons and bipolarons which have very low mobility and are limited in size by an elementary cell thus excluding coexistence with delocalized carriers (in contrast with the case of strong long-range EPI). As a result, the conductivity of systems with small polarons and bipolarons is orders of magnitude lower than that observed in cuprates. Besides, strongly ionic lattice of cuprates favors long-range (Frohlich) EPI [24]. Therefore, in the present article we consider systems with high density of correlated carriers and strong Frohlich EPI; the electron correlations that determine the band structure are taken into account in the effective mass approximation.

We have shown earlier that the ground normal state of a system with high carrier density and strong Fröhlich EPI is a two-component liquid where large bipolarons (whose size is much larger than the lattice constant) form charge ordering (CO) and coexist with delocalized carriers [6]. Parameters of this state in a compressible bipolaron fluid model were calculated with the variation method generalized to systems of interacting compressible bipolarons coexisting with delocalized carriers. The obtained [6] CO period and temperature of the CO (bipolarons) decay demonstrate the doping dependence, which is in accordance with experiments on cuprates. Earlier the two-component model has enabled to calculate the high-energy anomaly (“waterfall” and extremely broad features) observed in ARPES spectra of cuprates [25] being in quantitative agreement with experiments [7,12,13,26,27]. Spectrum of elementary excitations of the large-bipolaron liquid was calculated earlier [28]; the influence of the bipolaron liquid potential on delocalized carrier states as is shown below results in a pseudogap emergence.

Pseudogap is considered as display of absence of carrier states in some interval of energies under Fermi surface and in certain region of momentums near antinodes, i.e. in the vicinity of points  $(0, \pm\pi)$ ,  $(\pm\pi, 0)$ , observed in cuprates mainly with ARPES and STM methods [29-36]. It occurs at temperatures up to  $T^*$  which is higher than the temperature of superconducting transition, except overdoped systems [30]. To clarify the possible origin of the pseudogap in the present article we study an impact of potential created by large polarons and bipolarons (which we will denote below as CO potential) on delocalized Bloch states of carriers.

We look for stationary state of a delocalized carrier in presence of additional CO potential using Wannier theorem and dividing the medium into small regions having constant additional potential. The obtained new quasiparticle (QP) represents “distributed wave packet”. In such state the carrier wave vector is different in various regions of crystal due to variation of the additional CO potential. As we demonstrate, topology of cuprates-like dispersion does not allow propagation of such near-antinodal QPs. Nevertheless, photoelectrons caught in ARPES experiments can have near-antinodal wave vectors. This occurs when QPs with rather far from antinode average momentum escape from the regions with negative CO potential. The energy of antinodal photoelectrons is by the amplitude of the CO potential lower than that determined by the dispersion for their momentums.

These results are valuable as they allow to understand emergence of the pseudogap in ARPES and STM experiments as display of the revealed QP reconstruction in concert with cuprates-like dispersion. Namely, in ARPES spectra from the considered systems (i) the spectral weight is shifted to higher (in the absolute value) binding energies by the value of CO potential amplitude and (ii) spectral weight appears well below Fermi energy in rather wide interval of

wave vectors above the Fermi crossing. Finally, (iii) smearing of the carrier state over rather wide region of wave vectors results in great broadening of near-antinodal features. Just such peculiarities are observed in near-antinodal ARPES spectra of cuprates at  $T < T^*$  and disappear at  $T > T^*$  [31, 32]. Calculated earlier in the frames of the suggested model temperature of the CO onset [6] is in accordance with the experimental pseudogap onset temperature  $T^*$  including their doping dependence. Display of the found QP reconstruction in STM is also in agreement with experiments.

The article is organized as follows. In the Model and method section we describe the method of searching the stationary electron state in presence of additional CO potential and choose the model electron dispersion capturing the most important features of the dispersion in cuprates especially near Fermi energy in the near-antinodal region. In the Results and discussion section we first present two types of gaps in calculated transmission spectra. Then we study the QP reconstruction in presence of additional CO potential which in concert with cuprates-like dispersion results in pseudogap formation. After that we discuss display of this QP reconstruction in near-antinodal ARPES spectra and (briefly) in STM experiments. Conclusion contains summary and possible applications of the obtained results for further studies.

## 2. A model and methods

### 2.1. Combining Wannier theorem with a method reminiscent of finite elements method

We develop an approach to calculating the transmission coefficient for electrons propagating in the conduction plane modeling  $\text{CuO}_2$  plane in cuprates in an additional (to the lattice periodic potential) potential generated by bipolarons (or polarons, at very low doping). Potential created by bipolaronic CO (or unconventional charge density wave) for a carrier propagating in the conduction plane can be considered as a periodic function albeit with short coherence length. We model the additional potential energy of the electron due to CO presence (below we will briefly name it CO potential) with a simplest periodic function - a harmonic function:

$$U = U_0(\sin(K_{CO} x) + \sin(K_{CO} y)), \quad (1)$$

where  $K_{CO}$  is the wave vector of the CO determined in the considered model by the bipolaron radius  $R_{bip}$  as:  $K_{CO} x = K_{CO} y = 2\pi/(2R_{bip})$  [6]. We will consider CO potential amplitude  $U_0$  of the order of the pseudogap value in cuprates, as the pseudogap is just the energy necessary for an electron to make possible tunneling in an STM experiment. Then  $U_0$  is much smaller than the carrier bandwidth in cuprates. Zero average value of potential (1) is a consequence of electroneutrality.

As near-antinode electrons have one of two projections of the wave vector onto the conduction plane much larger than the other, we consider below the case  $k_x \gg k_y$  and initially neglect the change of the CO potential in y direction. We divide the conduction plane into  $N = N_p N_l + 1$  equal stripes parallel to y axis, where  $N_p$  is the number of the CO periods in the structure and  $N_l$  is the number of layers within one CO period, and average the bipolaron potential in each ( $j$ -th) layer over the CO period along y axis:

$$\langle U_j \rangle = \frac{U_0}{2R_{bip}} \int_0^{2R_{bip}} (\sin(K_{CO} x_j) + \sin(K_{CO} y)) dy = U_0 \sin(K_{CO} x_j) \quad (2)$$

The stripe width  $s$  is chosen so small that the potential can be considered constant in the limits of each stripe.

Let us consider Bloch electron with the energy  $\varepsilon$  and wave vector  $\mathbf{k}$  directed at the angle  $\alpha$  to  $x$  axis. The wave vector magnitude is determined by the energy  $\varepsilon$  according to the dispersion law  $\varepsilon(\mathbf{k})$ . Suppose that the electron meets a cluster of autolocalized charge carriers (polarons or bipolarons) described by the potential (2). According to Wannier theorem the Shroedinger equation for stationary electron state in the crystal periodic potential and additional potential  $\langle U_j \rangle$  (below we will omit angular brackets) which is small in comparison with the bandwidth can be written as

$$[\varepsilon(-i\nabla) + U_j]\Psi_j = E\Psi_j, \quad (3)$$

where  $\varepsilon(\mathbf{k})$  is Bloch electron dispersion having an extremum at  $\mathbf{k}_e=(k_{e,x}, k_{e,y})$  [37]. The effective mass method allows one to solve equation (3) using expansion of the electron dispersion near its extremum(s) (being interested in the hole-doping case, below we consider maximum(s)) up to the second order terms with standard definition of the effective mass  $m^*$  which is supposed isotropic below:

$$\varepsilon(\mathbf{k}) = \varepsilon(\mathbf{k}_e) + \frac{\hbar^2}{2m^*} [(k_x - k_{e,x})^2 + (k_y - k_{e,y})^2] \quad (4)$$

In the dispersion of hole-doped cuprates due to the symmetry of the conduction plane there are four maximums in the first Brillouin zone (FBZ). In the model dispersion used below we put them into the corners of the FBZ. Figure 1(a) demonstrates an example of the model dispersion in the first quadrant of the FBZ. Obviously, for cuprates-like dispersion the effective mass is not constant in the whole FBZ. However, for the present consideration it is enough if the effective mass is approximately constant in comparatively narrow region of energies  $E_F - U_0 < \varepsilon < E_F + U_0$  near Fermi energy. Then changing the wave vector of the carrier due to additional CO potential does not result in changing its effective mass. Figure 1(a) represents an example of paraboloid which yields such approximation for the model dispersion.

Equation (3) with using expansion (4) has the form

$$[\varepsilon(\mathbf{k}_e) + \frac{\hbar^2(-i\nabla - \mathbf{k}_e)^2}{2m^*} + U_j]\Psi_j = E\Psi_j \quad (5)$$

As the potential energy  $U_j$  is constant in each  $j$ -th stripe the solution of equation (5) has the form

$$\Psi_j = A_j e^{i\mathbf{k}_j \mathbf{r}_j} + B_j e^{i\mathbf{k}_j' \mathbf{r}_j}, \quad (6)$$

where  $\mathbf{k}_j = k_{j,x} \mathbf{e}_x + k_{j,y} \mathbf{e}_y$  is the wave vector of the incident electron wave in  $j$ -th stripe and  $\mathbf{k}_j' = -k_{j,x} \mathbf{e}_x + k_{j,y} \mathbf{e}_y$  is the wave vector of the reflected wave in the same stripe, they both are depicted in Figure 1(b),  $A_j, B_j$  are complex amplitudes of the incident and reflected waves, respectively. Due to the symmetry of the dispersion (which according to Landau theorem is determined by lattice symmetry) kinetic energy for incident and reflected waves in  $j$ -th layer coincides. Substituting (6) into (5) and then returning to the left-hand side in the dispersion expansion (4) one obtains equation that determines the wave vector modulus  $k_j$  in  $j$ -th stripe at given  $\alpha$ :

$$\varepsilon(\mathbf{k}_j) = E - U_j . \quad (7)$$

While  $U$  does not depend on  $y$  coordinate  $y$ -projection of the wave vector is conserved at the boundaries of the layers with constant potential:  $k_{j-1,y} = k_{j,y}$ , whereas  $x$  projection  $k_{j,x}$  changes its value according to equation (7). Of course, such approximation is more suitable near antinode where  $y$  projection of the wave vector is much shorter than its  $x$ -projection so that change of the potential along  $y$  axis during the carrier propagation may be initially neglected. Then we consider also the case where dependence of the CO potential on  $y$  coordinate is taken into account.

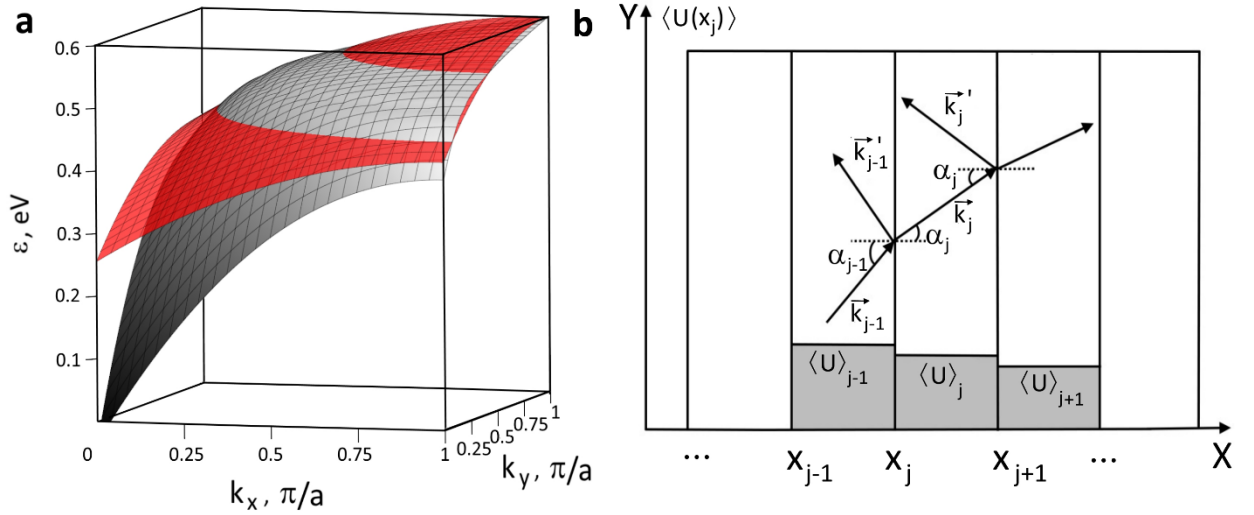


Fig. 1 (a) Grey surface represents an example of the carrier dispersion considered in the article (it is described by equation (12) with  $d=1.5$ ,  $c=1.5$ ,  $d'=0.65$ ,  $c'=0.13$ ), red surface is paraboloid  $\varepsilon = 0.6 - 0.26[(k_x - k_{e,x})^2 + (k_y - k_{e,y})^2]$ ,  $k_{e,x} = k_{e,y} = \pi/a$ , approximating the dispersion in the interval of energies  $0.48eV - U_0 < \varepsilon < 0.48eV + U_0$ ,  $U_0 = 0.05$  eV; (b) wave vectors of the incident and reflected electron waves in several layers with constant (in the layer) potential.

Let us calculate transmittance of the carrier waves in the layered structure described above. Standard boundary conditions relate carrier's wave functions in adjacent layers:

$$\begin{cases} \Psi_{j-1}(x_j, y_j) = \Psi_j(x_j, y_j) \\ \left. \frac{\partial \Psi_{j-1}}{\partial x} \right|_{x_j, y_j} = \left. \frac{\partial \Psi_j}{\partial x} \right|_{x_j, y_j} \end{cases}, \quad (8)$$

where  $x_j = x_{j-1} + s$ ,  $y_j = y_{j-1} + s * tg\alpha_j$ . System of Equations (8) relates amplitudes of the wave function in adjacent layers:

$$\begin{aligned} A_j &= \frac{1}{2} \left( 1 + \frac{k_{j-1,x}}{k_{j,x}} \right) e^{i(\mathbf{k}_{j-1} - \mathbf{k}_j) \cdot \mathbf{r}_j} A_{j-1} + \frac{1}{2} \left( 1 - \frac{k_{j-1,x}}{k_{j,x}} \right) e^{i(\mathbf{k}'_{j-1} - \mathbf{k}_j) \cdot \mathbf{r}_j} B_{j-1} \\ B_j &= \frac{1}{2} \left( 1 - \frac{k_{j-1,x}}{k_{j,x}} \right) e^{i(\mathbf{k}_{j-1} - \mathbf{k}_j) \cdot \mathbf{r}_j} A_{j-1} + \frac{1}{2} \left( 1 + \frac{k_{j-1,x}}{k_{j,x}} \right) e^{i(\mathbf{k}'_{j-1} - \mathbf{k}_j) \cdot \mathbf{r}_j} B_{j-1} \end{aligned} \quad (9)$$

Equations (9) can be written as follows

$$\begin{pmatrix} A_j \\ B_j \end{pmatrix} = \begin{pmatrix} a_j & b_j \\ c_j & d_j \end{pmatrix} \begin{pmatrix} A_{j-1} \\ B_{j-1} \end{pmatrix}$$

Then the system of  $N$  layers transforms the wave function amplitudes as the following matrix product:

$$\begin{pmatrix} A_N \\ B_N \end{pmatrix} = \begin{pmatrix} a_N & b_N \\ c_N & d_N \end{pmatrix} \begin{pmatrix} a_{N-1} & b_{N-1} \\ c_{N-1} & d_{N-1} \end{pmatrix} \dots \begin{pmatrix} a_2 & b_2 \\ c_2 & d_2 \end{pmatrix} \begin{pmatrix} A_1 \\ B_1 \end{pmatrix} = \begin{pmatrix} T_{11} & T_{12} \\ T_{21} & T_{22} \end{pmatrix} \begin{pmatrix} A_1 \\ B_1 \end{pmatrix}$$

Taking into account  $R = \left| \frac{B_1}{A_1} \right|^2$ ,  $R + D = 1$ , and  $D = \left| \frac{A_N}{A_1} \right|^2$ , where  $D$  is the total transmission coefficient, we come to quadratic equation for  $\beta = \sqrt{R}$ :

$$\beta^2(1 + |T_{12}|^2) + 2\beta(\text{Re}(T_{11})\text{Re}(T_{12}) + \text{Im}(T_{11})\text{Im}(T_{12})) + |T_{11}|^2 - 1 = 0 \quad (10)$$

Solving Equation (10) one obtains transmission  $D$  for any value of the electron energy  $E$  and angle  $\alpha$  between the wave vector  $\mathbf{k}$  and  $x$  axis.

Modeling change of the carrier wave vector at the carrier propagation in a CO potential depending on both  $x$  and  $y$  coordinates is carried out in a similar way. The square region of the crystal with the side  $CN_p$ , where  $C=2R_{bip}$  is the period of CO, is divided into square cells with the side  $s = C/N_l$ . The potential in each cell is considered constant calculated as follows

$$U_j = \frac{U_0}{2} * \left[ \sin\left(\frac{2\pi X_j}{c}\right) + \sin\left(\frac{2\pi Y_j}{c}\right) \right] \quad (11)$$

where  $X_j, Y_j$  are the coordinates of the bottom left angle of  $j$ -th cell. Comparison of the angle  $\alpha_j$  with the limiting angle  $\alpha_1(j) = \text{arctg}[(Y_j + y_j - s)/(X_j + x_j - s)]$  determines whether the refraction occurs on the cell boundary parallel to  $x$  axis or to  $y$  axis.

## 2.2. Modeling cuprates-like dispersion in the vicinity of Fermi energy

Our recent calculation revealed the gap in the spectrum of delocalized carriers caused by their scattering on the potential created by autolocalized carriers forming CO in the simplest model with one-dimensional periodic potential (that corresponds to antinodal direction of the carrier wave vector) and parabolic dispersion  $\varepsilon = \frac{\hbar^2}{2m^*} k_x^2$  [6]. The energetic position of the gap in that system depended on the CO period as the gap was caused by destructive interference of electron waves similarly to photon crystal effect. Here we consider carriers moving in arbitrary direction within the conduction plane (i.e. with arbitrary wave vectors in the 2D FBZ) and having dispersion close to that in cuprates (at least near Fermi energy and near antinode in the momentum space). The dispersion can be taken from that in ARPES spectra of cuprates since as was shown earlier [10] in systems with strong EPI it follows ‘‘bare’’ (i.e. in absence of EPI) carrier dispersion (shifted by the energy released at the system relaxation [25]).

Experimental ARPES data on cuprates show that width of the lower Hubbard band is about 0.5 - 0.6 eV [7] and the Fermi surfaces at different doping levels  $p$  typical of cuprates can be approximated by four 90-degree arcs of the circumferences [26,29]. In the first quadrant of

the FBZ considered below the center of the circumference is in (b,b) point, where  $b = \frac{\pi}{a}$ ,  $a$  is the lattice constant, as illustrated by figure 2. The circumference radius at zero doping is  $\tilde{k}_0 = b\sqrt{2/\pi}$  as follows from the condition of equality of the filled and unfilled areas in the FBZ at zero doping; at higher doping the arc radius  $\tilde{k} > \tilde{k}_0$ . We use tildes to mark that these vectors of the momentum space start in point (b,b). The wave vectors  $\mathbf{k}=(k_x, k_y)$  corresponding to points on the constant energy surface are simply related with  $\tilde{k}$ :  $\tilde{k}^2 = (k_x - b)^2 + (k_y - b)^2$ , as is illustrated by figure 2.

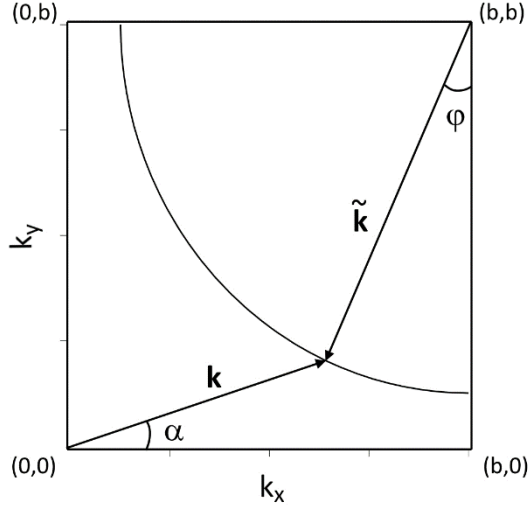


Figure 2. Relation between the wave vector  $\mathbf{k}$  and angle  $\alpha$  (between  $\mathbf{k}$  and x axis) and the vector  $\tilde{\mathbf{k}}$  and angle  $\varphi$ ; the arc of circumference is the constant energy surface,  $b=\pi/a$ .

We study several dispersion laws expressed by equation (12) with different  $d$  values from 1 to 2 that satisfy the conditions described above and are in rather good accordance with experimental dispersion in cuprates near the antinode and Fermi energy under hole doping  $p < 0.26$ :

$$\varepsilon = 0.5 - c * (\tilde{k} - \tilde{k}_0)^d, \tilde{k} > \tilde{k}_0, \quad \varepsilon = 0.5 + c' * (\tilde{k}_0 - \tilde{k})^{d'}, \tilde{k} < \tilde{k}_0, \quad (12)$$

Figure 3(a,b) represents dispersion (12) for  $d=1.2$  and  $1.5$ , respectively. For the comparison figure 3(c) demonstrates the dispersion (13) calculated for cuprates at low doping with holes [38] (with slightly modified coefficients)

$$\varepsilon = 0.34 - 0.18 \cos(k_x) \cos(k_y) - 0.08(\cos(2k_x) + \cos(2k_y)) \quad (13)$$

Unfortunately, dispersion (13) is not suitable for calculation of the angular dependence of the pseudogap as is discussed below.

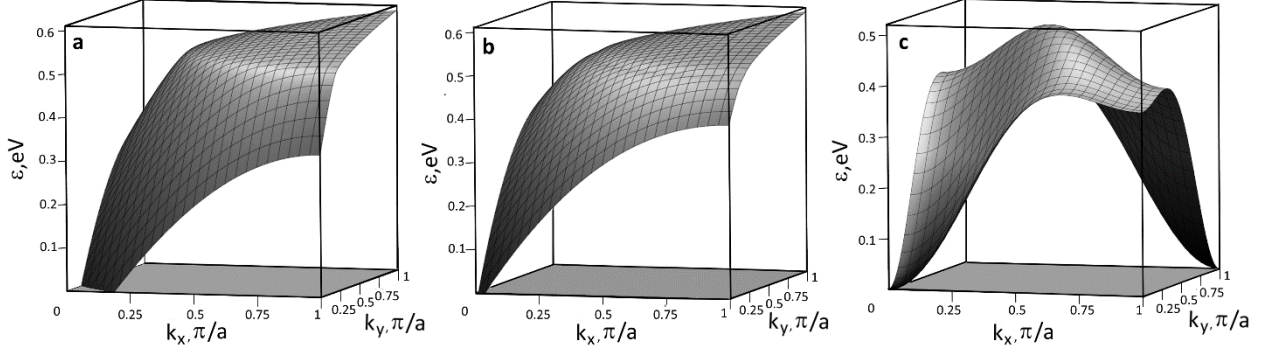


Figure 3 (a) and (b) Electron dispersion (12) with  $d=1.2$ ,  $c=1.5$ ,  $d'=0.65$ ,  $c'=0.13$  and  $d=1.5$ ,  $c=1.5$ ,  $d'=0.65$ ,  $c'=0.13$ , respectively; (c) electron dispersion (13).

To calculate the pseudogap width one needs Fermi energy value as function of doping. In the quasi-2D system considered here it is easily deduced from the equation relating the area  $S$  in  $k$ -space between the Fermi surfaces corresponding to zero and non-zero doping (shown with grey in figure 4(a,b)) and the surface density of doped holes  $n_h$ :  $S = (2\pi)^2 n_h / 2$ , where  $n_h = \frac{p}{a^2}$ ,  $p$  is the doping value, and 2 is due to spins. In the case of dispersion (12)  $S$  is the area between two curves, which are cross sections of the surface  $\varepsilon(\mathbf{k})$  by the planes  $\varepsilon(\mathbf{k}) = \varepsilon_F$  and  $\varepsilon(\mathbf{k}) = \varepsilon(\tilde{\mathbf{k}}_0)$ . By construction these curves are circumferences as shown by figure 4(a), and  $S$  is the area of a ring of the width  $\Delta\tilde{k} = \tilde{k}_F - \tilde{k}_0$ , where  $\tilde{k}_F = \sqrt{2\pi n_h + \tilde{k}_0^2}$ . Thus, for dispersion (12) Fermi energy as function of doping has the form  $\varepsilon_F(p) = 0.5 - c(\tilde{k}_F(p) - \tilde{k}_0)^d$ .

For dispersion (13) different constant-energy sections have different shapes, such as an ellipse or rectangle, as is seen from figure 4(b) dispersion (13) is unsuitable for studying the angular dependence of the pseudogap at small Fermi surface angles.

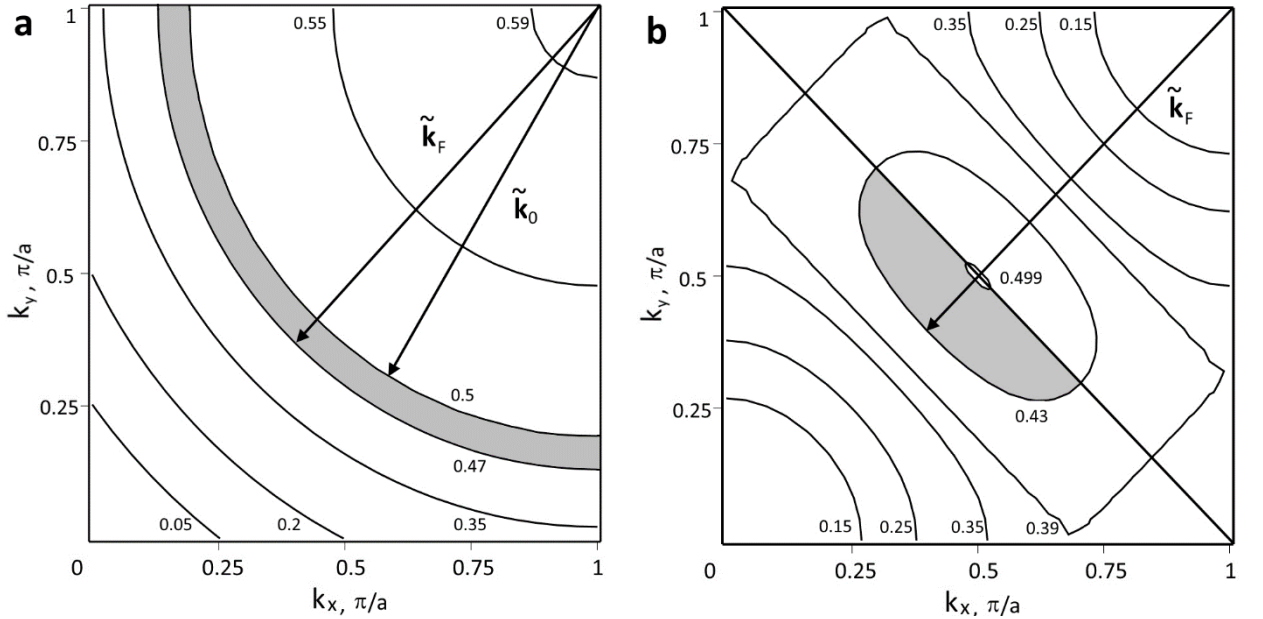


Figure 4 (a,b). Fermi energy determination from the area between the constant-energy curves for the case of doping  $p=0.2$ : (a) for dispersion (12) at  $d=1.5$ ,  $c=2$ ,  $d'=0.65$ ,  $c'=0.13$ , Fermi energy

changes from 0.499 eV at  $p=0.01$  up to  $\approx 0.458$  eV at  $p=0.25$ ; (b) for dispersion (13), Fermi energy changes from 0.496 eV at  $p=0.01$  up to 0.415 eV at  $p=0.25$ . Curves are the constant energy surfaces, numbers near the curves indicate energy values for each section. Gray regions depict the area  $S$ .

### 3. Results and discussion

#### 3.1. Gaps in calculated electron transmittance spectrum

In the frames of the developed approach let us study change in the transmittance spectrum of delocalized carriers due to presence of CO potential generated by autolocalized carriers. Figure 5 represents typical transmittance spectrum for electrons propagating in a crystal inside which there are  $N_p$  periods of the CO. As we checked, for the results it does not matter whether bipolarons form a single cluster or several clusters separated by regions with an absent or lower CO potential. We use below  $N_p = 100$ , the number  $N_l$  of layers per CO period where potential is considered constant  $N_l=32$ , changing both these parameters does not influence the results. The value of the CO potential amplitude  $U_0$  used is 0.05 eV. It was chosen as the value of the order of pseudogap in cuprates measured with ARPES and tunneling [31-36] since as will be seen below the pseudogap is approximately equal to the amplitude of the CO potential.

As is seen from figure 5, there are two gaps in the calculated transmission spectrum but only one of them is just below Fermi energy. The position of the lower-energy gap depends on the period of the CO potential. This dependence points out that the lower-energy gap is caused by destructive interference of waves scattered on the CO, similarly to the photon crystal effect. The higher-energy gap turns out to be pinned just below the Fermi energy and does not change with period of the CO potential (we will use below the CO period  $C=14\text{\AA}$  close to that observed in cuprates [39]). As will be demonstrated below it appears due to impossibility for the Bloch electron waves with the wave vectors near antinodes to propagate in crystal with CO potential and electron dispersion characteristic of cuprates. Since emergence of these gaps is not related with the superconductivity onset it is natural to call it pseudogap.

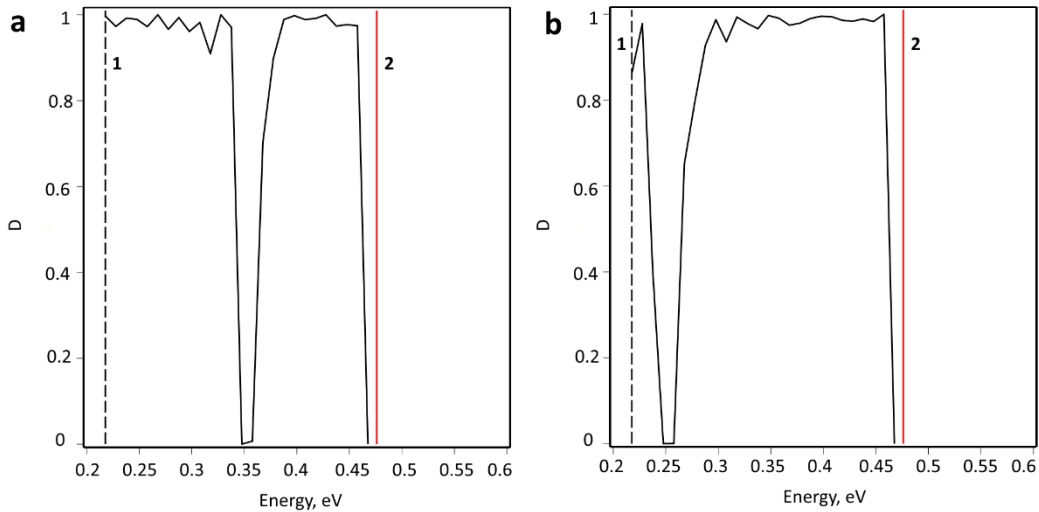


Figure 5 (a), (b). Calculated electron transmission spectra (black lines) for the dispersion (12) with  $d=1.2$ ,  $c=1.5$ ,  $d'=0.65$ ,  $c'=0.13$ ,  $U_0=0.05$  eV,  $N_p=100$ ,  $N_l=32$ ,  $\varphi=25^\circ$ ; in panel (a) the CO period  $C=13\text{\AA}$ , in panel (b)  $C=14\text{\AA}$ . Vertical red line 2 indicates Fermi energy  $E_F=0.476$  eV

corresponding to doping  $p=0.1$ , vertical dashed line 1 shows the minimum possible energy  $E_{min}=0.217$  eV of the electron for the angle  $\varphi$  used.

### 3.2. Quasiparticle reconstruction in presence of additional CO potential

Let us consider the origin of the found above pseudogap whose position does not change with CO period. Figure 6 demonstrates trajectories along which the wave vector of near-antinodal Bloch electrons changes at their propagation in additional CO potential (2). As the boundaries between the layers with constant potential are parallel to y axis, the y-projection of the wave vector  $k_y$  is conserved on each boundary:

$$k_{j,y} = k_j \sin \alpha_j = k_0 \sin \alpha_0 \quad (14)$$

where  $k_j$ ,  $\alpha_j$  и  $k_0$ ,  $\alpha_0$  are the modulus of the wave vector and the angle between it and x axis in  $j$ -th layer with the CO potential  $U_j$  and in a layer with zero CO potential, respectively. Let us note that to set a Bloch electron state in the considered 2D system one can determine either the wave vector projections  $(k_{x0}, k_{y0})$  or one of the values  $\tilde{k}$ ,  $E$ , or  $k_{y0}$  together with the angle  $\varphi_0$  (shown in figure 2) in a layer with zero CO potential. During propagation in additional CO potential the 2D electron wave vector (two its projections or the modulus and the angle with x axis) should satisfy the system of equations (7) and (14). Below we will use for  $\varepsilon(\mathbf{k})$  in equation (7) the dispersion (12), then equation (7) takes the following form (energy is in eV):

$$E - U_j = 0.5 - c * \left( \sqrt{(k_{j,x} - b)^2 + (k_{j,y} - b)^2} - \tilde{k}_0 \right)^d, E < 0.5,$$

$$E - U_j = 0.5 + c' * \left( \tilde{k}_0 - \sqrt{(k_{j,x} - b)^2 + (k_{j,y} - b)^2} \right)^{d'}, E > 0.5. \quad (15)$$

Thus, in the case of model dispersion (12) the QP wave vector should satisfy equations (14,15).

Geometrical analysis of compatibility of equations (14,15) illustrated by figure 6 turns out to be the most apparent. Obviously, with changing  $U_j$  at some total energy  $E_I$  characterizing the stationary state the left-hand side of equation (15) changes from  $\varepsilon=E_I-U_0$  to  $\varepsilon=E_I+U_0$ . Concurrently  $k_x$  value in the right-hand side should change at fixed  $k_y$  determined by the wave vector in layers with zero CO potential through (14). Let us consider trajectories in the momentum space of two near-antinodal Bloch electrons with the same total energy  $E_I$  and two different wave vectors in layers with zero CO potential which can be set also by specifying angles  $\varphi_1$  and  $\varphi_2$  on the constant energy surface  $\varepsilon=E_I$ . The first trajectory (line 1 in figure 6(a)) corresponding to larger angle  $\varphi_1$  reaches both the minimal kinetic energy surface  $\varepsilon=E_I-U_0$  (this occurs in the layers with the maximal CO potential, point A in figure 6(b)) as well as the maximal kinetic energy surface  $\varepsilon =E_I+U_0$  (in the layers with the minimal CO potential, point C in figure 6(b)). The second trajectory (line 2 in figure 6(a)) corresponding to smaller angle  $\varphi_2 < \varphi_1$  reaches the former surface but does not reach the latter.

Hence, at  $\varphi \geq \varphi_1$  there exist real roots of the system of equations (14,15) in each layer of the CO potential. Therefore, the states with the energy  $E_I$  and  $\varphi \geq \varphi_1$  are real quasiparticles (QP). One can note that distribution of the QP state over wave vectors is reminiscent wave packet. However, in this “distributed wave packet” the components with different wave vectors occur in

different layers of the coordinate space with different CO potential. Below we will classify the QP states according to their energy  $E$  (that determines the radius of the circumference arc in the momentum space) and angle  $\varphi_0$  in zero-potential layers and designate them  $(E, \varphi_0)$ . At  $\varphi_0 < \varphi_1$  and  $E = E_I$  there are no real roots of the system (14,15) in some layers with negative CO potential. As a result, the transmission vanishes for such electron states which correspond thus to virtual quasiparticles.

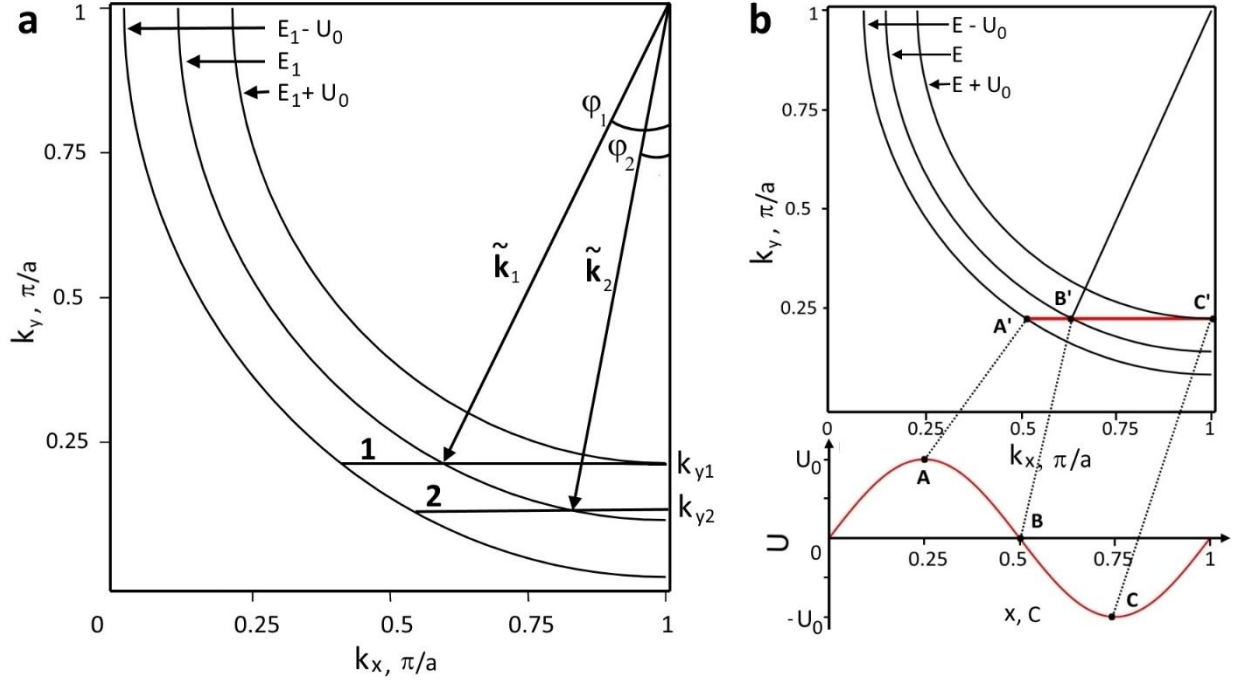


Figure 6 (a) Lines 1,2 depict trajectories of the carrier momentum at propagation in additional CO potential. While trajectory 1 reaches both maximum  $\varepsilon = E_I + U_0$  and minimum  $\varepsilon = E_I - U_0$  kinetic energy surfaces and, thus, correspond to real QPs, trajectory 2 does not reach the surface  $\varepsilon = E_I + U_0$ , therefore carrier state  $(E_I, \varphi_2)$  corresponds to virtual QP. (b) Structure of the new QP state (“distributed wave packet”): correspondence between points of trajectory in the momentum space and layers of the CO potential where the carrier has such momentum value.

Thus, negative half-wave of the CO potential caused by attraction of electrons to hole bipolarons together with topology of the constant energy surfaces characteristic of cuprates result in peculiarity of the near-antinodal QPs and, as will be demonstrated below, in the pseudogap emergence. It should be noted that, due to partial reflection of electron waves, besides the trajectory in the first quadrant of the FBZ shown in figure 6, complete momentum trajectory comprises the trajectory reflected in plane which is perpendicular to  $x$  axis and contains  $(0,0)$  point.

### 3.3. Manifestation of the QP reconstruction caused by CO potential in ARPES spectra

Let us consider how the revealed reconstruction of the stationary electron states occurring when the CO caused by strong EPI emerges in a system with cuprates-like dispersion displays

itself in ARPES spectra. Obviously, electron with given total energy  $E$  (which is equal to its kinetic energy  $\varepsilon$  only in layers with zero CO potential) can escape due to photoabsorption from areas with different CO potential  $U_j$  having, as a result, different values of the wave vector (i.e. different values of  $\varphi$ ) satisfying the equations (14, 15). This is illustrated in figure 6(b) depicting a trajectory of the wave vector of the electron QP and the values of the CO potential corresponding to some trajectory points.

The carrier state with some total energy  $E=E_I$  and  $\varphi_0=\varphi_2$  in figure 6(a), having y projection of the wave vector  $k_{y2}$ , is not real QP, as was discussed above. Therefore, it does not display itself in ARPES spectrum. The carrier with the energy  $E=E_I$  and  $\varphi_0=\varphi_1$  in figure 6(a) (having y projection of the wave vector  $k_{y1}$ ) is real QP. Its trajectory in the momentum space achieves the constant kinetic energy surface  $\varepsilon=E_I+U_0$  at the FBZ boundary, i.e. at  $\mathbf{k}=(b,k_{y1})$ :

$$\varepsilon(b,k_{y1})=E_I+U_0 \quad (16)$$

However, as is demonstrated by equation (16), the carrier total energy  $E_I$  is  $U_0$  lower than it is dictated by the dispersion for its instant momentum:  $E_I=\varepsilon(b,k_{y1})-U_0$ . Such carrier can absorb a photon, being in the layer with the minimum CO potential (point C in figure 6(b)). Then it displays itself in the ARPES spectrum at the momentum  $\mathbf{k}=(b,k_{y1})$  and binding energy  $E_I-E_F = \varepsilon(b,k_{y1})-U_0-E_F$ .

Thus, photoelectrons with the antinodal wave vectors  $\mathbf{k}=(b,k_y \leq k_{Fy})$  and corresponding to them (according to the dispersion law) binding energy  $\varepsilon(\mathbf{k})-E_F$ , ordinarily observed in normal metals and in cuprates at  $T>T^*$  (when CO vanishes), are absent in the considered system. Instead spectral weight near the FBZ boundary  $\mathbf{k}=(b,k_y \leq k_{Fy})$  appears at higher (by the CO potential amplitude) binding energy  $\varepsilon(\mathbf{k})-U_0-E_F$ . Such shift of the spectral weight to higher binding energies by approximately 0.05 eV in comparison with the spectrum taken at temperature  $T>T^*$  (when CO is absent), is indeed observed in the near-antinode ARPES spectra of optimally doped Bi2201 crystal at low temperatures in the whole interval of  $k_y \leq k_{Fy}$  [31,32]; this phenomenon is ordinarily named pseudogap.

Angular dependence of the pseudogap in the suggested approach is also in agreement with that observed in cuprates [29, 31-33]. At the antinode ( $\varphi=0$ ) the pseudogap width is  $U_0$  as discussed above. From the other hand, there exists the minimal value of  $\varphi_0$  corresponding to real QP with given energy. It marks closing the pseudogap and may be denoted as  $\varphi_{\text{clos}}$ . For example, in figure 6(a)  $\varphi_{\text{clos}}=\varphi_1$  provided  $E_F=E_I$ . Obviously, motion along the Fermi surface towards the increase of  $\varphi$  results in decreasing pseudogap from  $U_0$  at  $\varphi=0$  to zero at  $\varphi_{\text{clos}}$ . The value of  $\varphi_{\text{clos}}$  is related with dispersion parameters. Geometrical demonstration of this relation illustrated by figure 7(a) is again the most simple. For instance, let us find an example of the dispersion corresponding to  $\varphi_{\text{clos}}=30^\circ$  like it is observed in experiments on cuprates. To do this one should solve an equation

$$\tilde{k}(E)\cos 30^\circ = \tilde{k}'(E + U_0), \quad (17)$$

where  $\tilde{k}(\varepsilon)$  and  $\tilde{k}'(\varepsilon)$  are determined by the dispersion law (12) and shown in figure 7(a). For example, for  $p=0.15$  at  $d=1.2$ ,  $c=1.5$  and  $c'=0.1$  the solution of equation (17) yields  $d'=0.8$ . Figure 7(b,c) demonstrates the Fermi surface angle corresponding to pseudogap closing in systems with different dispersion parameters at various doping levels  $p$ .

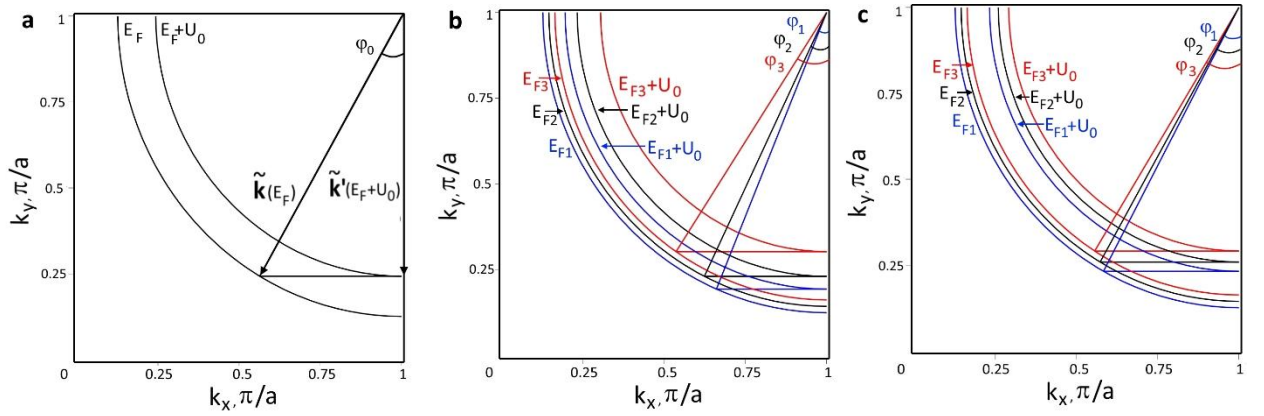


Figure 7 (a) The method to calculate the parameter  $d'$  in dispersion (12) corresponding to pseudogap closing at given Fermi-surface angle  $\phi_0$ , for example, at  $\phi_0=30^\circ$ ; (b, c) variation of the closing angle for different doping levels and dispersion parameters: in panel (b)  $d=1.2$ ,  $c=1.5$ ,  $d'=0.65$ ,  $c'=0.13$ ,  $E_{F1}(p=0.2)=0.447$ ,  $\phi_1=23^\circ$ ,  $E_{F2}(p=0.15)=0.461$ ,  $\phi_2=26^\circ$ ,  $E_{F3}(p=0.1)=0.476$ ,  $\phi_3=33.6^\circ$ ; in panel (c)  $d=1.5$ ,  $c=1.5$ ,  $d'=0.4$ ,  $c'=0.12$ ,  $E_{F1}(p=0.2)=0.477$ ,  $\phi_1=28.5^\circ$ ,  $E_{F2}(p=0.15)=0.485$ ,  $\phi_2=30^\circ$ ,  $E_{F3}(p=0.1)=0.492$ ,  $\phi_3=32^\circ$ .

Surprisingly, the experimental low-temperature near-antinode ARPES spectra [31-33] demonstrate also rather large spectral weight in a wide interval of the wave vectors above Fermi crossing ( $k_y > k_{Fy}$ ) but at energies essentially below Fermi energy. Often this phenomenon is interpreted as display of QPs interference. To substantiate this conclusion the supposition about back-bending of the energy dispersion curves (EDC) is used [40], although from the alternative point of view this “back-bending” is a result of gradual vanishing the spectral weight (which is clearly seen when it is depicted in the form of image plots [31]) depicted in the form of EDCs. However, even besides arisen discussion is it back-bending or saturation in experimental EDCs [40], another divergence of such picture with experimental EDC is evident. Namely, the width of the EDC features at any  $k_y < k_{Fy}$  is very large, comparable with the binding energy in the maximum [31,32]. Obviously, it hardly can be interpreted as Bogolyubov QP with certain momentum and energy as it is supposed in PDW model based on Amperian pairing [41]. Such giant broadening clearly points out to breaking the picture of Bloch or Bogolyubov QPs having certain energy and momentum as anticipated in literature [40]. In the model under study the source of giant broadening is smearing the QP over wide region of momentums considered in the next Section where dependence of the CO potential on both x and y coordinates is taken into account.

The appearance of spectral weight at  $k_y > k_{Fy}$  near antinode in the present approach originates naturally from the described above shift of the spectral weight by the CO potential amplitude to higher binding energies (caused by the QP reconstruction and dispersion topology near antinode). For the photoelectron from the antinode with the wave vector corresponding to Fermi crossing ( $b, k_y = k_{Fy}$ ) the binding energy is not zero but  $-U_0$  as is demonstrated above. Dispersion near antinode in cuprates is flat, as is seen, for example, from the ARPES spectrum (EDC) of optimally doped Bi2201 at temperature  $T > T^*$  shown in figure 2(a) in [32]. Therefore the spectral weight maximum in EDCs taken at  $k_x = b$ ,  $k_y > k_{Fy}$  occur approximately at the same binding energy  $-U_0$  excluding narrow interval near the “end point”  $k_{y\max}$  corresponding to the Fermi surface angle  $\phi_{\text{clos}}$  where the pseudogap closes. In the experimental antinodal EDCs taken for several wave vectors along lines parallel to  $k_y$  axis at  $k_x \approx b$  (lines C1, C2 in figures 1,2 in the

article [32]) the “end point” lies out of the interval of the wave vectors depicted. EDC corresponding to as high  $k_y$  as  $k_{y\max}$  is represented only for line C7 [32] which is also parallel to  $k_y$  axis but intersects the Fermi surface at  $\varphi$  about  $30^\circ$ .

### 3.5. Model with CO potential depending on both x and y coordinates and broadening of ARPES features.

Let us now study a more general model of the CO without averaging the potential (1) over y coordinate. We still consider near-antinodal carriers but now we take into account that propagating Bloch waves face also boundaries parallel to x axis (in the present approach all boundaries are chosen to be parallel to the coordinate axes). As a result, their trajectories in the momentum space cease to be horizontal lines and consist of horizontal and vertical small steps enclosed in quasi-rectangles exemplified by figure 8. As is seen from figure 8(c), trajectories of near-antinodal carriers in the momentum space achieve the surfaces of the higher and lower kinetic energy approximately along diagonal of the quasi-rectangle, the angle between the diagonal and the x axis can be approximated with  $\alpha$ . Thus, one can again obtain geometrical estimation of the dispersion parameters providing the pseudogap closing at any Fermi surface angle  $\varphi_0$ . Besides  $\varphi_0$ , the equation will include  $k_{x0}$  value shown in figure 8(c), although for rough estimation one can use dispersion parameters satisfying the equation (17) with  $\varphi_0$  instead of  $30^\circ$ .

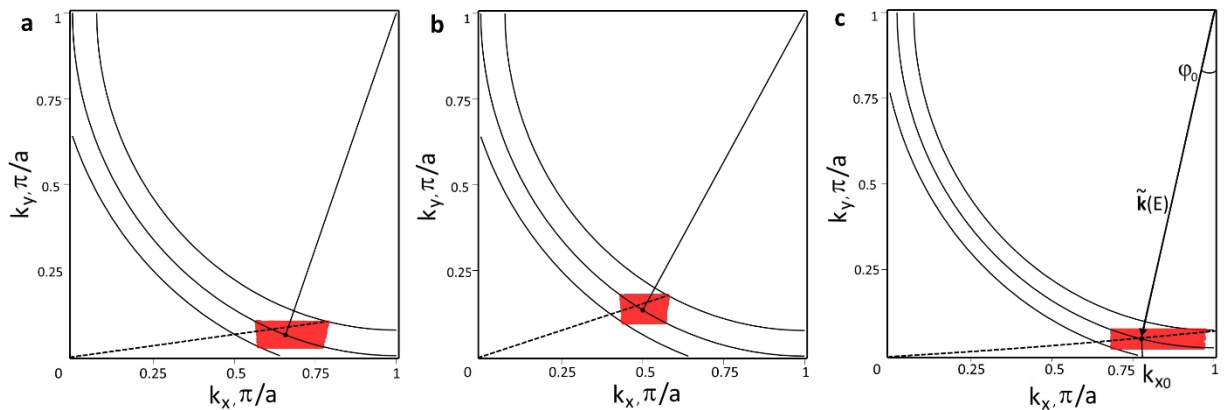


Figure 8. Trajectories of the electron wave vector at propagation in CO potential depending on both x and y coordinates with the amplitude  $U_0=0.05$  eV,  $N_p=100$ ,  $N_l=32$ . In panel (a)  $d=1.5$ ,  $c=1.5$ ,  $E=0.4$  eV,  $\varphi_0=20^\circ$ ; in panel (b)  $d=1.5$ ,  $c=1.5$ ,  $E=0.4$  eV,  $\varphi_0=30^\circ$ ; in panel (c)  $d=1.2$ ,  $c=1.5$ ,  $E=0.35$  eV,  $\varphi_0=\varphi_{\text{clos}}=13.2^\circ$ .

In the frames of the suggested approach with a model CO potential depending on both x and y coordinates giant broadening of the EDC maximums in ARPES spectra emerges naturally as it is illustrated by figure 9 (a,b). It represents “trajectories” of the carrier momentum for two carriers, whose energies  $E_1$  and  $E_2$  in zero-potential layers differs by more than  $U_0$ . The trajectory regions intersect or touch each other, therefore photoelectrons with the momentum from the intersection of red and blue regions can have any energy from the interval  $[E_1, E_2]$  which is wider than  $U_0$ . Similar broadening is demonstrated by near-antinodal spectral weight in ARPES spectra of cuprates at  $T < T^*$  [31,32]. Temperature  $T^*$  of the pseudogap emergence in cuprates [31,32] is in agreement with CO emergence temperature calculated in the model with strong Frohlich EPI [6]. It should be noted that complete trajectories of the carrier momentum in

the model with 2D CO potential apart of those shown by figures 8,9 comprise also ones reflected in planes containing  $k_x$  or  $k_y$  axes and perpendicular to the  $(k_x, k_y)$  plane.

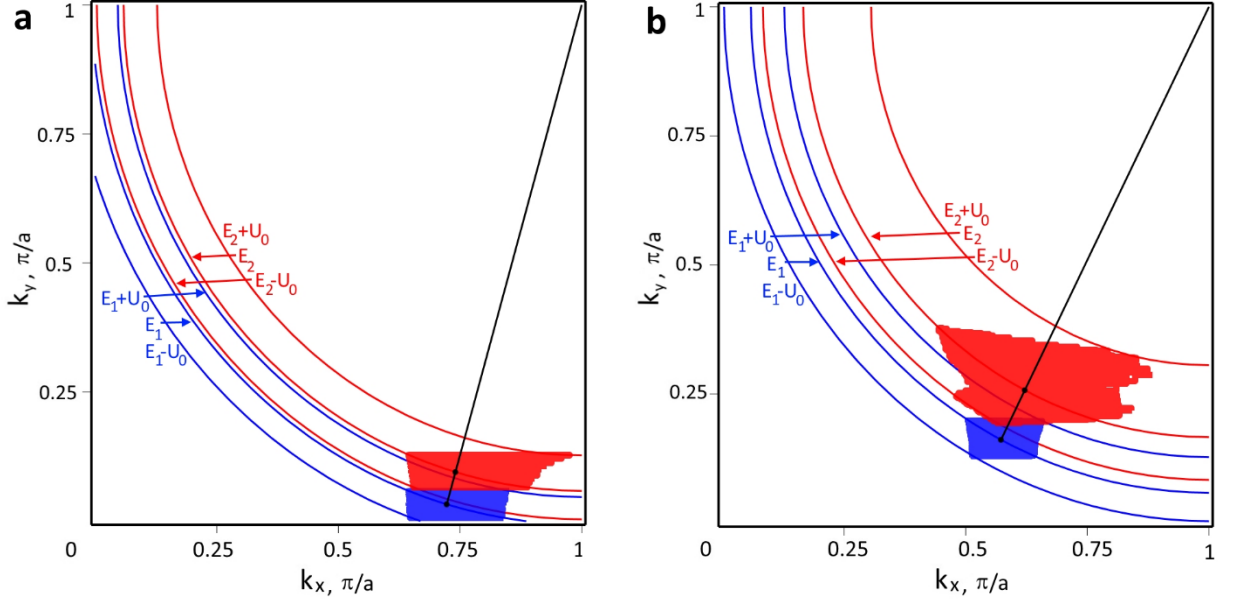


Figure 9 (a),(b) Illustration of the origin of ARPES features broadening. Blue and red areas are trajectories (at propagation in 2D CO potential) of the momentum for QPs with the same  $\varphi_0$  but different energies  $E_1$  and  $E_2$ , respectively,  $E_2 - E_1 > U_0$ . Photoelectron escaping from crystal with the wave vector lying on the boundary between red and blue regions can have any energy from the interval  $[E_1, E_2]$  whose width is larger than  $U_0$ . For both panels  $d=1.5$ ,  $c=2$ ,  $d'=0.65$ ,  $c'=0.2$ ,  $N_p=100$ ,  $N_f=32$ ; in panel (a)  $\varphi_0=16$ ,  $E_1=0.36$  eV,  $E_2=0.42$  eV; in panel (b)  $\varphi_0=27$ ,  $E_1=0.42$  eV,  $E_2=0.49$  eV.

### 3.5. Displaying QP reconstruction caused by CO potential in STM spectra.

Finally let us briefly discuss display of the described QP reconstruction in scanning tunneling microscopy (STM) which is the other basic experimental method of the pseudogap study. At considering the topographic map mode in the frames of the model under study the bias is superimposed on negative or positive CO potential in different regions of the surface. This results in variation of the tip height necessary for constant tunneling current, thus visualizing the charge distribution, that is apparently seen in experiments [34-36]. In the suggested approach there is not a necessity to suppose inhomogeneity due to dopant ions as is often used in interpretation of the topographic map obtained on cuprates [36].

Considering differential conductance, it is convenient to start from tunneling current of ordinary metal-metal contact written in the frames of Bardeen formalism [42,43]:

$$I = \frac{2\pi e}{\hbar} \sum_{\mu, \nu} f(E_\mu) [1 - f(E_\nu + eV)] |M_{\mu\nu}|^2 \delta(E_\mu - E_\nu) \quad (18)$$

where  $E_\mu$  and  $E_\nu$  are energies of the states  $\psi_\mu$  and  $\psi_\nu$  in the probe and on the surface, respectively, and  $f(E)$  is Fermi function. If  $\psi_\nu$  is a state of the system considered above which is different from ordinary Fermi-liquid, the factor  $[1-f(E_\nu+eV)]$  in (18) should be replaced with the density of states on the surface available for filling in the suggested approach. Obviously, it gradually increases with the voltage  $V$  up to its value  $U_0/e$ , since near-antinodal states are initially (at zero bias) unavailable due to presence of negative half-wave of the CO potential. With the increase of bias, they become available for carriers that acquire lacking energy (which varies from 0 up to  $U_0$  for states with different “angular distance” to the antinode) due to the bias. Thus, compensating negative part of the CO potential by the carrier energy  $eV$  in the applied field results in increasing density of available states. Such increase of differential conductance (representing density of available states) with increasing bias up to pseudogap width value is observed in experiments on cuprates [34-36].

#### 4. Conclusion

In summary, we report the QPs reconstruction emerging in a doped system with strong long-range EPI due to CO potential and its role in pseudogap formation in ARPES and STM spectra of systems with cuprates-like dispersion. We reveal that topology of cuprates-like dispersion makes impossible propagation of near-antinodal QPs. Photoelectrons with antinodal momentums stem from QPs with average momentums rather far from antinode when they escape from areas with minimal (negative) CO potential. Therefore the energy of such photoelectrons is by the CO potential amplitude lower than that dictated by dispersion for their momentum. As a result, spectral weight in ARPES spectra is shifted to higher (in the absolute value) binding energy forming pseudogap and greatly broaden. Angular dependence of the pseudogap obtained is in good agreement with experimental results. Besides, the approach predicts spectral weight at momentums above the Fermi crossing but with energies well below the Fermi energy which is observed in ARPES spectra of cuprates.

Apart of ARPES spectra preliminary estimation of displaying the revealed QP reconstruction in STM spectra shows agreement with experimental studies of pseudogap in cuprates. Temperature of the CO decay (due to bipolarons thermal decay) in systems under study calculated earlier as function of doping [6] is consistent with doping dependence of the temperature  $T^*$  of the pseudogap disappearance in cuprates. Thus, we have demonstrated that in systems with strong long-range EPI and high density of carriers with dispersion typical of cuprates the peculiarities in the ARPES and STM spectra ordinarily unified under pseudogap title occur due to QP reconstruction in presence of CO potential. Earlier in the frames of the model with strong Frohlich EPI the nodal ARPES spectra were calculated with taking into account joint relaxation of coupled systems [25], and they turn out to be in quantitative agreement with nodal-direction ARPES spectra in cuprates including high-energy anomaly and great linewidth. Strong Frohlich EPI results also in CO formed by large polarons (at lower carrier density) and bipolarons, whose period and onset temperature are in agreement with those observed in cuprates [6].

The results obtained show that strong Frohlich EPI not only convert states of carriers with the low energy into autolocalized ones but due to this conversion induces transformation of delocalized QP states into distributed wave packets. From one hand the findings of the article stress the importance of strong EPI in doped cuprates that is pointed out also in many other

theoretical and experimental studies [3-11,14-17,21-25,28]. From the other hand our results change the idea about QP states in doped cuprates. The QP reconstruction revealed may be useful in interpreting results of STM, Andreev reflection, spectroscopic imaging STM and plethora of other similar experiments in cuprates. It possibly also could help to shed light on a well-known enigma of peak-dip-hump structure in ARPES and STM spectra [29,35].

## Acknowledgments

We are grateful to A. S. Mishchenko, D. Emin and S. G. Ovchinnikov for valuable communication. The work was supported by Southern Federal University

## References

- [1] Bozovic I and Ahn C 2014 *Nat. Phys.* **10** 892
- [2] Keimer B, Kivelson S A, Norman M N, Uchida S and Zaanen J 2015 *Nature* **518** 179
- [3] Lanzara A *et al* 2001 *Nature* **412** 510
- [4] Le Tacon M *et al* 2014 *Nat. Phys.* **10** 52
- [5] Reznik D *et al* 2006 *Nature* **440** 1170
- [6] Myasnikova A E, Nazdracheva T F, Lutsenko A V, Dmitriev A V, Dzhantemirov A H, Zhileeva E A and Moseykin D V 2019 *J. Phys.: Condens. Matter* **31** 235602
- [7] Zhu J X, McElroy K, Lee J, Devereaux T P, Si Q, Davis J C and Balatsky A V 2006 *Phys. Rev. Lett.* **97** 177001
- [8] Ronning F, Shen K M, Armitage N P, Damascelli A, Lu D H, Shen Z-X, Miller L L and Kim C 2005 *Phys. Rev. B* **71** 094518
- [9] Shen K M *et al* 2004 *Phys. Rev. Lett.* **93** 267002
- [10] Emin D 1995 *Phys. Rev. B* **52** 13874
- [11] Mishchenko A S and Nagaosa N 2004 *Phys. Rev. Lett.* **93** 036402
- [12] Rösch O, Gunnarsson O, Zhou X J, Yoshida T, Sasagawa T, Fujimori A, Hussain A, Shen Z-X and Uchida S 2005 *Phys. Rev. Lett.* **95** 227002
- [13] Xie B P *et al* 2007 *Phys. Rev. Lett.* **98** 147001
- [14] Valla T, Kidd T E, Yin W-G, Gu G D, Johnson P D, Pan Z-H and Fedorov A V 2007 *Phys. Rev. Lett.* **98** 167003
- [15] Myasnikova A E and Myasnikov E N 2008 *Phys. Rev. B* **77** 165136
- [16] Lupi S, Nicoletti D, Limaj O, Baldassarre L, Ortolani M, Ono S, Ando Y and Calvani P 2009 *Phys. Rev. Lett.* **102** 206409
- [17] Bastiaans K M, Cho D, Benschop T, Battisti I, Huang Y, Golden M S, Dong Q, Jin Y, Zaanen J & Allan M P 2018 *Nature Physics* **14** 1183
- [18] Wang Q Y *et al* 2012 *Chin. Phys. Lett.* **29** 037402
- [19] Ge G F *et al* 2015 *Nat. Mater.* **14** 285
- [20] Miyata Y, Nakayama K, Sugawara K, Sato T, Takahashi T 2015 *Nat. Mater.* **14** 775
- [21] Song Q *et al* 2019 *Nature Comm.* **10** 758
- [22] Hague J P, Kornilovitch P E, Samson J H and Alexandrov A S 2007 *Phys. Rev. Lett.* **98** 037002
- [23] Makarov I A, Shneyder E I, Kozlov P A and Ovchinnikov S G 2015 *Phys. Rev. B* **92** 155143
- [24] Emin D 2013 *Polarons* (Cambridge: Cambridge University Press)
- [25] Myasnikova A E, Zhileeva E A and Moseykin D V 2018 *J. Phys.: Condens. Matter* **30** 125601
- [26] Graf J *et al* 2007 *Phys. Rev. Lett.* **98** 067004

- [27] Moritz B et al 2009 *New J. Phys.* **11** 093020
- [28] Emin D 2015 *Phil. Mag.* **95** 918
- [29] Damascelli A, Hussain Z, Shen Z-X 2003 *Rev. Mod. Phys.* **75** 473
- [30] Hübner S, Hossain M A, Damascelli A and Sawatzky G A 2008 *Reports on Progress in Physics* **71** 062501
- [31] Hashimoto M et al 2010 *Nat. Phys.* **6** 414
- [32] He R-H et al 2011 *Science* **331** 1579
- [33] Hashimoto M, Vishik I M, He R-H, Devereaux T P and Shen Z-X 2014 *Nat. Phys.* **10** 483
- [34] Lang K M, Madhavan V, Hoffman J E, Hudson E W, Eisaki H, Uchida S and Davis J C 2002 *Nature* **415** 412
- [35] Fischer Ø, Kugler M, Maggio-Aprile I, Berthod C, Renner C 2007 *Rev. Mod. Phys.* **79** 353
- [36] Fujita K, Schmidt A R, Kim E-A, Lawler M J, Lee D H, Davis J C, Eisaki H and Uchida S J 2012 *J. Phys. Soc. Jpn.* **81** 011005
- [37] Luttinger J M and Kohn W 1955 *Phys. Rev.* **97** 869
- [38] Dagotto E 1994 *Rev. Mod. Phys.* **66** 763
- [39] Comin R and Damascelli A 2016 *Ann. Rev. Condens. Matter Phys.* **7** 369
- [40] Agterberg D F et al 2020 *Ann. Rev. Condens. Matter Phys.* **11** 231
- [41] Lee P A 2014 *Phys. Rev. X* **4** 031017
- [42] Bardeen J 1961 *Phys. Rev. Lett.* **6** 57
- [43] Tersoff J and Hamann D R 1985 *Phys. Rev. B* **31** 805